DOI: 10.1002/ejic.200600731

A Ligand-Driven Geometry Switch in Octahedral and Trigonal-Bipyramidal Iron Complexes Containing (H)PNO and PNN Ligands

Paolo Pelagatti,*[a] Alessia Bacchi,[a] Marcella Balordi,[a] Andrea Caneschi,[c] Marco Giannetto,[a] Corrado Pelizzi,[a] Luca Gonsalvi,[b] Maurizio Peruzzini,[b] and Franco Ugozzoli[a]

Keywords: Iron / N,P ligands / Ligand effects

Complexation reactions of Fe^{II} and Fe^{III} salts with the tridentate ligands 2-(diphenylphosphanyl)benzaldehyde benzoylhydrazone [(H)PNO] and *N*-[2-(diphenylphosphanyl)benzylidene]-2-(2-pyridyl)ethanamine (PNN) was carried out. For (H)PNO, reaction of a stoichiometric amount of anhydrous $FeCl_2$ in the presence of a primary alcohol such as MeOH, EtOH or *n*BuOH gave the mixed-valence Fe^{II}/Fe^{III} paramagnetic complex $[Fe\{\kappa^3\text{-}(H)PNO\}_2]Cl[FeCl_4]$, whereas the reaction between $FeCl_2$ and a twofold excess of (H)PNO in the presence of AgOTf (OTf = triflate, OSO_2CF_3) led to the isolation of the bis-chelate paramagnetic ferrous complex $[Fe\{\kappa^3\text{-}(H)PNO\}_2][OTf]_2$. A diamagnetic bis-chelate ferrous complex $[Fe\{\kappa^3\text{-}(PNO)_2\}]$ was instead obtained from the reaction of $FeCl_2$ with a twofold excess of (H)PNO in the presence of NaOMe. In the case of the PNN ligand, the 1:1 reaction with $FeCl_2$ gave the neutral paramagnetic trigonal-bipyramidal complex $[Fe(\kappa^3\text{-PNN})Cl_2]$. The X-ray structures of $[Fe\{\kappa^3\text{-}(H)PNO\}_2]Cl[FeCl_4]$, $[Fe_2\{\kappa^3\text{-}(H)PNO\}_2Cl_6]$ and $[Fe(\kappa^3\text{-PNN})Cl_2]$ are reported, together with CV and magnetic susceptibility measurements and an ab initio study aimed at rationalizing the different stoichiometries and structures observed with the two tridentate ligands.

Introduction

The interest in five-coordinate iron(II) complexes with tridentate ligands stems mainly from their high catalytic activity in olefin polymerisation. The most active and studied systems are those containing the 2,6-bis(arylimino)-pyridyl moiety (NNN ligands),[1] although examples with ONN[2] and PNP[3] ligands have also been reported. Recently, cobalt complexes containing tridentate ligands have also been combined with iron to create mixed-valence and heterometallic [2 × 2] grid-like arrays,[4] spin-crossover complexes,[5] models of enzyme active sites such as catechol dioxygenases[6] and nitrile hydratase,[7] and asymmetric sulfide oxidation catalysts.[8] Some of us have been involved in the study of the coordinating behaviour of asymmetric tridentate ligands towards transition metals for several years.[9] The most thoroughly investigated ligand, 2-(diphenylphosphanyl)benzaldehyde benzoylhydrazone [(H)-PNO, Scheme 1], has been used to synthesise Pd^{II} and Ru^{II} complexes that are active catalysts in alkene hydrogenation[10] and addition of benzoic acid to terminal alkynes,[11] respectively. The importance of the iron complexes containing the Fe(LLL) moiety (LLL = tridentate ligand) prompted us to investigate the coordinating behaviour of (H)PNO towards $FeCl_2$. This study was subsequently extended to another tridentate ligand, namely *N*-[2-(diphenylphosphanyl)benzylidene]-2-(2-pyridyl)ethanamine (PNN),[12] which bears a 2-(2-aminoethyl)pyridine function

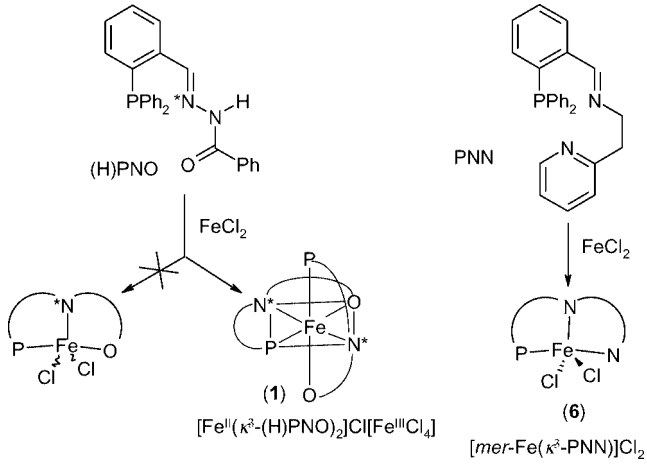

Scheme 1. The anions of complex **1** have been omitted.

[a] Dipartimento di Chimica Generale ed Inorganica, Chimica Analitica, Chimica Fisica, Università degli Studi di Parma, Viale G.P. Usberti 17/A, 43100 Parma, Italy
E-mail: paolo.pelagatti@unipr.it
[b] Istituto di Chimica dei Composti OrganoMetallici, Consiglio Nazionale delle Ricerche (I.C.C.O.M.), Via Madonna del Piano 10, 50019 Sesto Fiorentino, Firenze, Italy
[c] Dipartimento di Chimica & UdR INSTM, Università degli Studi di Firenze, Via della Lastruccia 3, Polo Scientifico, 50019 Sesto Fiorentino, Firenze, Italy

instead of an (H)NC(O)Ph arm (Scheme 1). The ligand PNN differs from HPNO as it is aprotic and forms two six-membered chelate rings instead of a six- and a five-membered chelation ring as for (H)PNO upon complexation.

In this paper we describe the synthesis and full characterisation of a series of iron complexes obtained by reaction between (H)PNO and anhydrous $FeCl_2$ or hydrated $FeCl_3$ and PNN and anhydrous $FeCl_2$. The X-ray structures of $[Fe\{\kappa^3\text{-(H)PNO}\}_2]Cl[FeCl_4]$ (**1**), $[Fe_2\{\kappa^3\text{-(H)PNO}\}_2Cl_6]$ (**2**) and *mer*-$[Fe(\kappa^3\text{-PNN})Cl_2]$ (**6**) are also reported. A rationalisation of the different stoichiometries and geometries observed for the iron complexes with the two tridentate ligands is also provided on the basis of ab initio calculations.

Results and Discussion

Complexes Containing HPNO

Tridentate aroyl hydrazones easily form iron complexes containing the octahedral entity $[FeL_2]^{n+}$ (L = tridentate aroyl hydrazone, n = 0, 2 or 3), where the charge depends on the anionic or neutral character of the ligands as well as on the oxidation state of the metal. These complexes, which are usually synthesised by employing an L:Fe molar ratio of 2:1, are generally very stable, and aroyl hydrazones are in fact being studied as sequestrating agents for the treatment of iron overload diseases.[13] As octahedral bis-chelate complexes are usually considered to be ineffective in catalysis, our first aim was to isolate five-coordinate iron(II) species of the type *mer*-$[Fe\{\kappa^3\text{-(H)PNO}\}Cl_2]$ (Scheme 1) with a trigonal-bipyramidal or square-pyramidal geometry. Therefore, we initially treated a dichloromethane solution of (H)PNO with a stoichiometric amount of anhydrous $FeCl_2$ dissolved in *n*-butanol[14] at room temperature. The reaction gave a purple solid of formula *mer*-$[Fe\{\kappa^3\text{-(H)PNO}\}_2]Cl[FeCl_4]$ (**1**) in good yield. The same product could also be isolated by carrying out the reaction at reflux in other alcohols such as MeOH or EtOH, by reverting the sequence of addition of the reagents, or by adding the ligand-containing solution dropwise to the alcoholic solution of the iron salt. The use of neat thf as solvent as well as an (H)PNO:$FeCl_2$ molar ratio of 1:5 did not change the reaction course either. Complex **1** contains the ferrous cationic fragment $[Fe\{\kappa^3\text{-(H)PNO}\}_2]^{2+}$, the tetrahedral tetrachloroferrate anion $[FeCl_4]^-$ and a free chloride ion (Scheme 1).

Two ligands bind to the iron(II) ion in a neutral tridentate fashion through the phosphorus, the imine nitrogen and the amide oxygen in the octahedral cation. The neutral character of the (H)PNO ligands is indicated by a weak IR stretching band at 3255 cm^{-1} for the N–H groups, while a single band at 1607 cm^{-1} indicates that both C=O groups are involved in the coordination.[9a,9g] The FAB(+) spectrum shows the presence of the fragment m/z = 1070 belonging to the cation $[\{Fe(HPNO)_2\}\{FeCl_4\}]^+$. Another intense cluster signal is centred at m/z = 871 belonging to the fragment $[Fe\{(H)PNO\}(PNO)]^+$, while a signal at m/z = 463 accounts for the fragment $[Fe(PNO)]^+$. In the ESI(+) spectrum of a methanol solution of **1**, the signal generated by the loss of the Cl^- is absent, while the cluster at m/z = 871 is well visible. Importantly, the ESI(–) spectrum shows a signal at m/z = 198 due to the $[FeCl_4]^-$ anion.

The electronic spectrum of an acetonitrile solution (10^{-7} M) of **1** shows the following bands in the region 250–1000 nm: 261 (ε = 55483 $M^{-1}cm^{-1}$), 306 (39774), 357 (29000) and a broad absorption band at 518 nm (7081). The bands at 261, 306 and 518 nm are typical of bis-chelate Fe^{II} complexes containing tridentate benzoylhydrazones, and are attributed to LMCT processes.[15] The absorption peak at 357 nm can be tentatively assigned to the $[FeCl_4]^-$ anion.[16] The alternative formula $[Fe^{III}\{\kappa^3\text{-(H)PNO}\}_2]Cl[Fe^{II}Cl_4]$ for complex **1** is unlikely because of the sensitivity of the $[FeCl_4]^{2-}$ anion to air[16a] and because of the soft character of the (H)PNO ligand (due to the phosphane moiety), which is expected to stabilize Fe^{II}. A further confirmation comes from the voltammetric measurements. Figure 1 shows the cyclic voltammogram of compound **1** (third of three scans) recorded in acetonitrile solution: the anodic signal at about +0.0025 V and the cathodic wave at about –0.2 V can be assigned, respectively, to the oxidation of the complexed Fe^{II} to Fe^{III} and the corresponding reduction back to Fe^{II}. The weak signal at about 0.75 V is ascribable to the ligand, which was also characterised by means of the same technique. The potential values observed for the Fe^{II}/Fe^{III} couple are, in fact, unusual for uncomplexed iron, such as $FeCl_4^-$ counterions. Moreover, cyclic voltammetric measurements carried out on a freshly prepared solution of anhydrous $FeCl_3$ in acetonitrile, under the same experimental conditions employed for the studied complex, show a system of anodic and cathodic signals at potential values above +0.250 V.

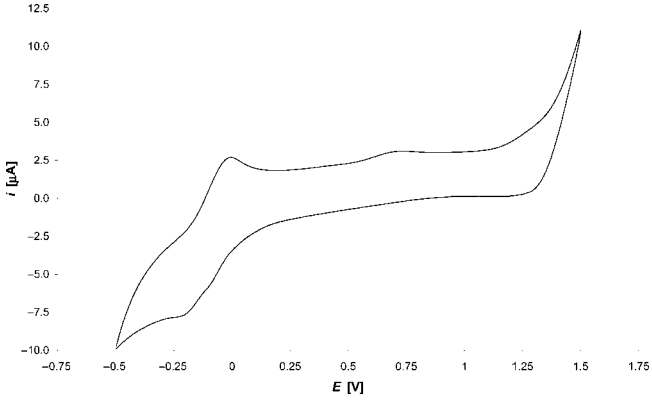

Figure 1. Cyclic voltammogram of compound **1** (third of three scans) recorded in acetonitrile solution. Scan rate: 0.1 $V s^{-1}$.

The ^1H NMR spectrum of **1** shows very broad signals in the 300–233 K temperature range owing to the presence of the paramagnetic $[FeCl_4]^-$ anion. However, the $^{31}P\{^1H\}$ NMR spectrum recorded at 300 K shows a singlet at δ = 63.4 ppm, as expected for two magnetically equivalent phosphorus nuclei in the complex cation. The paramagnetic character of **1** is evidenced by its magnetic behaviour. χT vs. T data were recorded in the range 50–300 K with an applied field of 1 T, where the zero-field splitting contri-

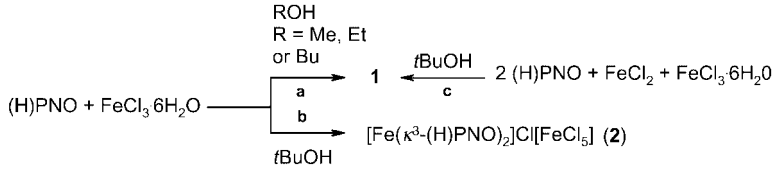

Scheme 2.

bution is not attended and saturation effects should not be yet present. These data show a Curie behaviour of around 4.2 emu mol K^{-1} in the whole temperature range, quite close to the expected $S = 5/2$ value for an isolated spin with $g = 2.0$ (4.375 emu mol K^{-1}).

Complex **1** was also obtained by treating (H)PNO with $FeCl_3 \cdot 6H_2O$ in methanol or ethanol at 80 °C, as confirmed by X-ray diffraction analysis on a single crystal isolated from the mother liquor and by IR and UV spectroscopy and elemental analysis (Scheme 2, pathway a). The X-ray structure of **1** is shown in Figure 2, where the Cl^- and $[FeCl_4]^-$ anions have been omitted for clarity.

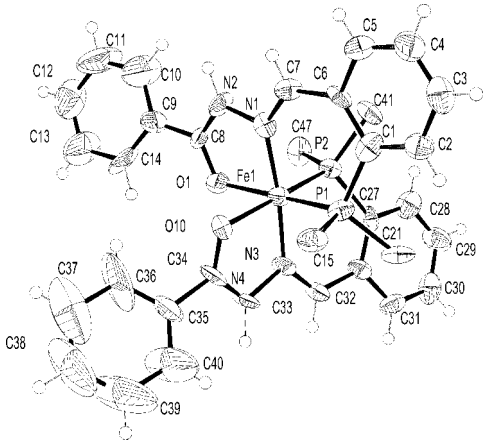

Figure 2. Perspective view and labelling scheme of *mer*-[Fe{κ^3-(H)-PNO}$_2$]$^{2+}$ in **1**. Thermal ellipsoids are shown at the 50% probability level. Phenyl groups C16–C20 (at C15), C22–C26 (at C21), C42–C46 (at C41), C48–C52 (at C47) have been omitted for clarity. A Cl^- and a $FeCl_4^-$ complete the structure.

Table 1 lists the main bond lengths and angles for **1**. The conformation of the two ligands is almost identical, and the complex shows a non-crystallographic symmetry around a twofold axis bisecting the O1–Fe1–O10 and the P1–Fe1–P2 angles. The PNO coordination forms a five-membered and a six-membered chelation ring for each ligand. In both cases the former is planar within 0.06 Å, while in the latter the P atom deviates significantly (0.5 Å) from the average plane defined by the remaining five atoms; this deformation is characteristic of most instances of coordinated 2-(diphenylphosphanyl)benzaldehyde hydrazones.[9g] However, even taking into account the out-of-plane deformation involving the P atoms, the overall conformation of the ligand backbone is planar within 0.30 Å. This feature will be a matter for comparison with complex **6**. The steric crowding of the diphenylphosphanyl groups belonging to the two ligands in the bis-chelate coordination induces intramolecular parallel stacking (3.5 Å) between the benzaldehyde aromatic ring of each ligand and one free phenyl of the other ligand. The complex cations are bridged by Cl^- anions through the hydrogen bonds N4–H···Cl5 [N···Cl = 3.04(1) Å; N–H···Cl = 160(10)°] N2–H···Cl5(x, 0.5 – y, 0.5 + z) [N···Cl = 3.10(5) Å; N–H···Cl = 154(6)°] to form a chain motif (Figure 3, left).

Table 1. Bond lengths [Å] and angles [°] for **1** and **6**.

1		**6**	
Fe1–N3	1.88(1)	Fe–N2	2.1083(3)
Fe1–N1	1.90(1)	Fe–N1	2.241(3)
Fe1–O10	1.971(9)	Fe–Cl1	2.294(1)
Fe1–O1	1.979(9)	Fe–Cl2	2.329(1)
Fe1–P2	2.232(4)	Fe–P	2.541(1)
Fe1–P1	2.249(4)		
N3–Fe1–N1	173.4(5)	N2–Fe–N1	86.7(1)
N3–Fe1–O10	82.3(5)	N2–Fe–Cl1	119.79(9)
N1–Fe1–O10	92.7(5)	N1–Fe–Cl1	91.80(9)
N3–Fe1–O1	92.7(5)	N2–Fe–Cl2	113.78(8)
N1–Fe1–O1	82.1(5)	N1–Fe–Cl2	91.35(8)
O10–Fe1–O1	80.0(4)	Cl1–Fe–Cl2	126.43(5)
N3–Fe1–P2	92.2(4)	N2–Fe–P	80.96(8)
N1–Fe1–P2	91.9(3)	N1–Fe–P	167.33(8)
O10–Fe1–P2	168.6(3)	Cl1–Fe–P	96.82(4)
O1–Fe1–P2	90.4(3)	Cl2–Fe–P	90.97(3)
N3–Fe1–P1	92.2(3)		
N1–Fe1–P1	92.1(4)		
O10–Fe1–P1	90.0(3)		
O1–Fe1–P1	168.1(3)		
P2–Fe1–P1	100.2(2)		

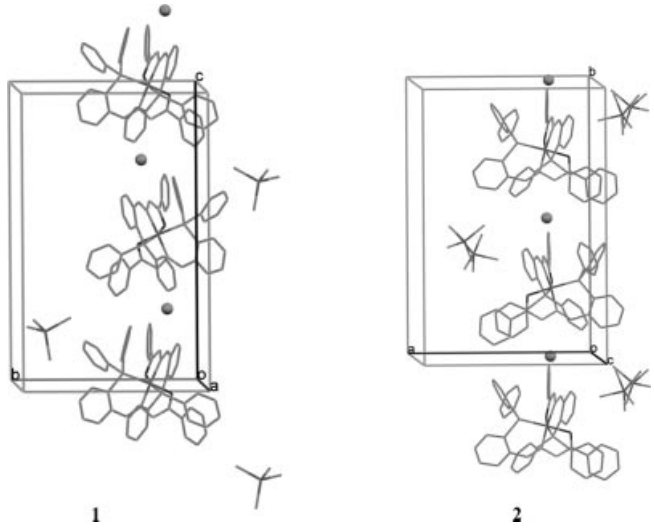

Figure 3. Comparison of the packing arrangements of **1** (left) and **2** (right), oriented so that axes of similar lengths correspond. The 60:40 disorder of $FeCl_4^{2-}$ and $FeCl_5^{2-}$ anions is shown in **2**.

The formation of **1** from the ferric salt clearly requires the presence of a reductant; since no traces of oxidized ligand were detected or isolated [two possible oxidative processes could involve the (H)PNO ligand: oxidation of the phosphane moiety to the corresponding phosphane oxide or oxidation of the aroyl hydrazone to diacyl hydrazine[13a]], the oxidation of the primary alcohols to the corresponding aldehyde must be invoked. The oxidation of primary alcohols promoted by Fe^{III} species is a rather uncommon process which, to the best of our knowledge, has been reported only rarely.[16a,17] Regrettably, repeated attempts to detect the expected aldehydes failed. However, the in situ iron(III) → iron(II) reduction was proved by treating (H)PNO with $FeCl_3·6H_2O$ and $FeCl_2$ in a 2:1:1 molar ratio in a *t*BuOH/CH_2Cl_2 mixture heated at reflux. The reaction gave complex **1** in high yield and purity, as demonstrated by the IR, UV and FAB mass spectra and microanalysis. Moreover, when the reaction between (H)PNO and $FeCl_3·6H_2O$ was repeated under reflux in a tertiary alcohol, such as *t*BuOH, which cannot undergo oxidative processes, a complex containing two Fe^{III} nuclei of stoichiometry $[Fe_2\{\kappa^3\text{-}(H)PNO\}_2Cl_6]$ (**2**) formed, as evidenced by elemental analysis (Scheme 2, pathway b).

Unfortunately, the mass (FAB and ESI) and IR spectra are not informative as they are identical to those of **1**. Cyclic voltammograms of complex **2** show a pattern comparable to **1**. This behaviour can be explained by considering that Fe^{III} is initially reduced to Fe^{II} in the first stage of the scan, starting from –0.5 V. The tendency to undergo reduction shown by the octahedral Fe^{III} centre in **2** explains the similarity of the mass spectra of complexes **1** and **2**, since redox processes can occur during such analysis.[18]

Crystals of **2** suitable for X-ray diffraction analysis were collected from the mother liquor. Compound **2**, with stoichiometry $[Fe_2\{\kappa^3\text{-}(H)PNO\}_2Cl_6]$, contains the $[Fe\{\kappa^3\text{-}(H)PNO\}_2]^{3+}$ cation, one chloride anion, and an apparent mixture of $[FeCl_4]^{2-}$ and $[FeCl_5]^{2-}$ anions disordered over two sites 3.7 Å apart (Figure 3, right).

The Fourier map of the region occupied by the complex anions was interpreted in terms of a substitutional disorder where some $[FeCl_4]^{2-}$ replaces the $[FeCl_5]^{2-}$ anions in a 60:40 proportion, even though this would imply a reduction of $[FeCl_5]^{2-}$, whose oxidized products have not been detected. The same disorder pattern was found when repeating the structure determination on crystals grown from different batches. Due to structural disorder and to the consequent poor quality of the refinement, the geometry of the trivalent bis-chelate cation is not significantly different from the divalent one crystallised with pure $[FeCl_4]^-$ in **1** and therefore does not allow us to assign unequivocally the oxidation state of the Fe atom based uniquely on the comparison of the Fe–P distances. The structure is based on chains of cations bridged by chloride anions via N–H···Cl hydrogen bonds; in both cases these chains are aligned along the 21 Å axis, which, however, has different symmetry properties in the two crystals (Table 3). These result in an array of heterochiral complexes generated by a *c* glide in **1** and in a homochiral chain generated by a 2_1 screw axis in **2**. In fact, the presence of a relevant amount of $[FeCl_5]^{2-}$ causes a remarkable rearrangement of the symmetry elements between the two compounds accompanied by a repositioning of the complex anions, which occupy different sites along the chains in the two cases (Figure 3).

When a methanol solution of anhydrous $FeCl_2$ was treated with a twofold excess of (H)PNO dissolved in dichloromethane at reflux, a purple solid of formula $[Fe\{\kappa^3\text{-}(H)PNO\}_2]Cl_2$ (**3**) was obtained (Scheme 3).

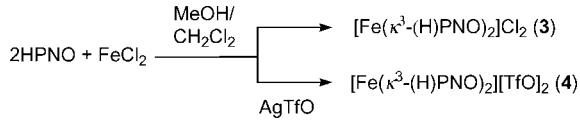

Scheme 3.

The ESI(+) mass spectrum of **3** shows a unique cluster centred at *m*/*z* = 871 due to the octahedral unit $[Fe\{(H)PNO\}(PNO)]^+$. The electronic spectrum does not show the band at 357 nm while the charge-transfer absorptions at 261, 306 and 507 nm are well visible. The IR spectrum shows a weak stretching band at 3220 cm^{-1}, which is indicative of the protic character of the ligands, whereas a band at 1603 cm^{-1} confirms that the C=O groups of the two PNO ligands are both involved in the coordination. Broad and uninformative bands are present in the ^1H NMR spectrum recorded at 300 K, while the $^{31}P\{^1H\}$ NMR spectrum shows a singlet at δ = 64.4 ppm that is compatible with the presence of the octahedral cation $[Fe\{\kappa^3\text{-}(H)PNO\}_2]^{2+}$; a small singlet at δ = 36.8 ppm is also visible, probably due to the partial oxidation of the phosphane P-atom of the (H)PNO ligand. On lowering the temperature to 233 K, the ^1H NMR signals do not sharpen. Careful inspection of the solid showed a substantial heterogeneity, as evidenced by the presence of differently coloured agglomerates (from red to deep purple). Regrettably, repeated recrystallisations did not improve the analytical quality of the product leading, in some cases, to decomposition and, in general, to irreproducible elemental analyses. On the basis of magnetic susceptibility measurements, the paramagnetic character of **3** seems imputable to traces of iron(III) species, probably due to aerobic oxidation. A rough evaluation of the χT versus T value in the temperature range 50–300 K with an applied field of 1 T for compound **3** gives a coarse percentage of about 10% of noninteracting iron(III) versus diamagnetic iron(II).

A clearer picture was obtained by treating (H)PNO with $FeCl_2$ in the presence of silver triflate; the removal of the chlorides led to the smooth formation of the bis-chelate complex $[Fe\{\kappa^3\text{-}(H)PNO\}_2][OTf]_2$ (**4**; Scheme 3). The reaction occurred with precipitation of silver chloride, which was separated by filtration to leave a red solution, from which a red powder was isolated. In this case, the elemental analysis is in agreement with the expected stoichiometry. The ESI(+) mass spectrum of a dichloromethane solution of **4** shows a cluster centred at *m*/*z* = 1021, corresponding to the loss of a triflate anion, and a second cluster centred at *m*/*z* = 871, corresponding to the fragment $[Fe\{(H)$

PNO}(PNO)]$^+$. The UV spectrum does not show the band at 357 nm, as expected due to the absence of the $[FeCl_4]^-$ anion. The IR spectrum agrees with the presence of two neutral (H)PNO ligands bound to the metal, as indicated by the stretching bands of the N–H and C=O groups at 3198 and 1605 cm^{-1}, respectively. The presence of the triflate anion is testified by intense IR bands at 1027 cm^{-1} [$\nu_s(SO_3)$], 1157 cm^{-1} [$\nu_{as}(CF_3)$], 1238 cm^{-1} [$\nu_s(CF_3)$] and 1296 cm^{-1} [$\nu_{as}(SO_3)$].[19] The ^{1}H NMR spectrum indicates a paramagnetic character of the complex, as inferred by the broad bands observed even at 233 K, while the $^{31}P\{^1H\}$ NMR spectrum shows a unique sharp signal at δ = 62 ppm, even at room temperature, as expected for two magnetically equivalent P nuclei. The cyclic voltammograms of complex **4** show a quite different behaviour with respect to complex **1** as these complexes contain different counterions. The presence of the triflate anion shifts both the anodic and cathodic peaks to potential values above +0.75 V. A higher value of ΔE_p (difference between anodic peak potential and cathodic peak potential) is also detected. These phenomena could be interpreted by considering the possibility that, in complex **1**, the metallic centre contained in the $[FeCl_4]^-$ counterion is actively involved in the electron-transfer mechanism of the coordinated iron.[20]

It is well known that a reinforced ligand–metal interaction favours a high crystal-field separation and leads preferentially to low-spin complexes that, in the case of d^6 metals in an octahedral environment, are diamagnetic. With the aim of isolating a neutral diamagnetic octahedral complex of the type [Fe(κ^3-PNO)$_2$] (**5**), a dichloromethane solution of (H)PNO was at first treated with a stoichiometric amount of NaOMe dissolved in methanol and the NaPNO salt thus formed was treated with a methanol solution of anhydrous $FeCl_2$ (ligand/metal = 2:1; Scheme 4).

$$2(H)PNO + FeCl_2 \xrightarrow[NaOMe]{MeOH/CH_2Cl_2} [Fe(\kappa^3\text{-}PNO)_2]\ (\mathbf{5})$$

Scheme 4.

The elemental analysis of the isolated purple solid agrees with the expected stoichiometry and the CI mass spectrum shows an intense cluster at m/z = 871 corresponding to [**5**+H]$^+$. The absence of the IR stretching bands of the N–H and C=O groups indicates that the two deprotonated ligands bind iron in an anionic PNO tridentate fashion. Measurements of the magnetic susceptibility at an applied magnetic field of 1 T suggest that the complex is diamagnetic in the temperature range 10–300 K. However, the ^{1}H NMR spectrum of a $CDCl_3$ solution of **5** recorded at 300 K contains very broad signals, which sharpen on lowering the temperature to 233 K. At this temperature the C(H)=N proton resonates at δ = 9.42 ppm as a singlet, while a doublet is observed at δ = 7.71 ppm ($^3J_{H,H}$ = 7.05 Hz) due to the two phenyl protons adjacent to the C=O group of the benzoyl function. The $^{31}P\{^1H\}$ NMR spectrum recorded at 233 K shows a singlet at δ = 69.2 ppm and a small singlet at around δ = –17 ppm. The first signal corresponds to the two magnetically equivalent P nuclei of the two coordinated (H)PNO ligands, while the more shielded singlet is indicative of a partial decoordination of a phosphorus. Because complex **5** is diamagnetic at 300 K, the broadening of the ^{1}H NMR lines at this temperature must be caused by molecular motions in solutions, which are absent at 233 K. Because the broadening involves the entire ^{1}H NMR spectrum, the fluxionality seems to be due to the decoordination and subsequent re-entering of the P (as further indicated by $^{31}P\{^1H\}$ NMR spectroscopy) and N-imine donors in the coordination sphere. This can reasonably be imputed to the isomerisation between the two Δ and Λ isomers that are expected to coexist in solution.

A Complex Containing the PNN Ligand

Substitution of the (H)NC(O)Ph arm with the 2-(2-aminoethyl)pyridine function certainly makes the ligand PNN more flexible than (H)PNO. This allows for different coordination modes, such as *mer*-κ^3-PNN with Pd^{II}[12,21] and Rh$^{I–III}$,[22] *fac*-κ^3-PNN or κ^2-PN with Cr, Mo and W,[23] μ-κ^3-PNN and even μ-κ^4-PNCN with Os clusters.[24] The reaction between equimolar amounts of anhydrous $FeCl_2$ and PNN in a $MeOH/CH_2Cl_2$ mixture at room temperature led to the isolation of the trigonal bipyramidal complex [*mer*-Fe(PNN)Cl$_2$]·1/2CH_2Cl_2 (**6**; Scheme 1) in good yield. The complex is a paramagnetic orange crystalline solid. The IR spectrum shows a shift of the IR stretching band of the C(H)=N moiety with respect to the free ligand, from 1653 to 1629 cm^{-1}, which is indicative of a Fe–N(imine) coordination. The FAB(+) mass spectrum shows a high degree of fragmentation of the analyte, which does not allow any simple interpretation. However, after amplification of the signal a small cluster at m/z = 63, corresponding to **6**, becomes visible. The structure of complex **6** was confirmed by single-crystal X-ray analysis. The tridentate PNN ligand in **6** occupies two apical and one equatorial sites of a trigonal bipyramidal coordination, which is completed by two Cl$^-$ ligands at the remaining equatorial sites (Figure 4). Table 1 lists the main bond lengths and angles for **6**. The tridentate coordination of PNN to the metal generates two six-membered chelation rings whose conformation is highly puckered, in contrast to the almost planar geometry observed for the coordination of (H)PNO in **1**. The ring formed by chelation of N1 and N2 is best described as a half-chair with the vector N2–C8 twisted relative to the ring plane (Cremer and Pople[25] puckering coordinates: Q_T = 0.56 Å, ϕ2 = –91°, θ2 = 44°), while the ring defined by chelation of N2 and P1 is intermediate between half-boat and a twisted chair, with a major displacement of P and Fe from the average ring plane (puckering coordinates: Q_T = 0.95 Å, ϕ2 = 149°, θ2 = 117°). The dramatic distortion from planarity observed in **6** is a consequence of the enlargement of the chelate ring by replacement of the hydrazonic arm of (H)PNO with a CH_2CH_2N system in PNN. The insertion of the ethyl segment in the chelate ring is necessarily accompanied by a deviation of C9 out of the local plane de-

fined by C6, C7, N2 and C8 around the iminic double bond. Consequently, the pyridine attached to C9 is rotated relative to the iminic plane (P–Fe–N2–C7 = 43°), and the phosphane group on the other side of the molecule is constrained to follow this rotation in order to maintain the *trans* geometry for the P–Fe–N1 angle. The overall molecular deformation of **6** relative to the planar tridentate chelation observed in **1** can be viewed as a rotation of the apical axis P–Fe–N1 of the coordination polyhedron around the hinge represented by the Fe–N2 vector. A similar deformation, with P–M–N=C torsion angles ranging between 17° and 44°, has been observed in the four other occurrences of complexes containing the PNN ligand[12,23a,26] characterised in the solid state.

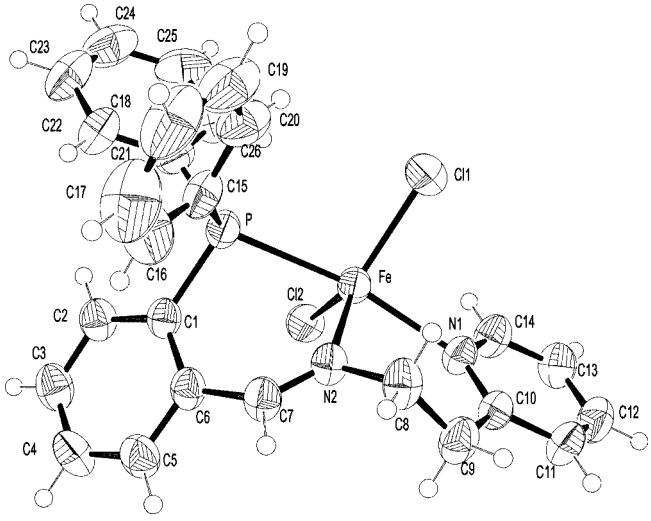

Figure 4. Perspective view and labelling scheme of *mer*-[Fe(κ^3-PNN)Cl_2] in **6**. Thermal ellipsoids are shown at the 50% probability level.

Modelling

To clarify the reasons for the formation of the octahedral cation $[Fe\{\kappa^3\text{-}(H)PNO\}_2]^{2+}$ rather than the analogous cation $[Fe(\kappa^3\text{-}PNN)_2]^{2+}$, we have undertaken theoretical calculations to predict and then to investigate their molecular structures.

The optimised geometries of the two ions were obtained by ab initio calculations using the semi-empirical PM3 method[27] in the Spartan 04 program[28] and are illustrated in Figure 5. The calculated bond lengths and angles in the five- and six-membered chelate rings are collected in Table 2. The results of the calculations indicate that the distances are consistent with the values reported in the literature. However, although the Fe–P distance in the $[Fe\{\kappa^3\text{-}(H)PNO\}_2]^{2+}$ ion (2.264 Å) falls just in the middle of the range observed from a perusal of the data available in the CSD (from 2.2 to 2.3 Å), the analogous distance calculated from the $[Fe(\kappa^3\text{-}PNN)_2]^{2+}$ ion (2.413 Å) is significantly longer and, to the best of our knowledge, is unprecedented in the solid-state structures reported in the CSD file.

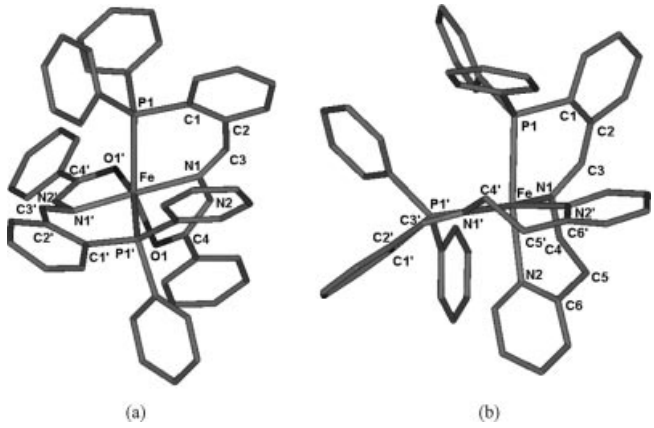

Figure 5. Optimised geometries obtained for the two cationic fragments $[Fe\{\kappa^3\text{-}(H)PNO\}_2]^{2+}$ (a) and $[Fe(\kappa^3\text{-}PNN)_2]^{2+}$ (b). Hydrogen atoms have been omitted for clarity.

This suggests that the increase of the Fe–P bond lengths in $[Fe(\kappa^3\text{-}PNN)_2]^{2+}$ compared to that in $[Fe\{\kappa^3\text{-}(H)PNO\}_2]^{2+}$ may be the reason why formation of the former cationic fragment is not observed. To further investigate this aspect we have studied in detail the electron density distribution along the Fe–P bond in the two cations. This was done by comparing the molecular isodensity surfaces in the two fragments at the same electron density value (for a large series of electron density values). We observed that the elec-

Table 2. Bond lengths and angles in the optimised geometries of the $[Fe\{\kappa^3\text{-}(H)PNO\}_2]^{2+}$ and $[Fe(\kappa^3\text{-}PNN)_2]^{2+}$ complexes obtained with the semi-empirical PM3 method. The distances between primed atoms are identical to those between unprimed ones (see Figure 5).

$[Fe\{\kappa^3\text{-}(H)PNO\}_2]^{2+}$				$[Fe(\kappa^3\text{-}PNN)_2]^{2+}$			
Bond lengths [Å]		Bond angles [°]		Bond lengths [Å]		Bond angles [°]	
Fe–P1	2.264	P1–Fe–O1	156.1	Fe–P1	2.413	P1–Fe–N4	171.8
Fe–N1	1.9	N1–Fe–P1	81.9	Fe–N1	1.941	N1–Fe–P1	83.5
Fe–O1	1.976	O1–Fe–N1	75.3	Fe–N2	1.944	N4–Fe–N1	92.7
P1–C1	1.828	Fe–P1–C1	107.7	P1–C1	1.845	Fe–P1–C1	105.3
C1–C2	1.4	P1–C1–C2	121.3	C1–C2	1.396	P1–C1–C2	116.8
C2–C3	1.461	C1–C2–C3	127.8	C2–C3	1.460	C1–C2–C3	128.6
C3–N1	1.307	C2–C3–N1	128.6	C3–N1	1.311	C2–C3–N1	132.6
N1–N2	1.463	C3–N1–Fe	137.7	N1–C4	1.485	C3–N1–Fe	133.2
N2–C4	1.401			C4–C5	1.517		
C4–O1	1.261			C5–C6	1.489		
				C6–N2	1.377		

tron density along the Fe–P bond is much larger in $[Fe\{\kappa^3\text{-}(H)PNO\}_2]^{2+}$ than in $[Fe(\kappa^3\text{-}PNN)_2]^{2+}$. Figure 6 shows, as an example, that two voids in the electron density along the two Fe–P bonds in $[Fe(\kappa^3\text{-}PNN)_2]^{2+}$ are evident in the molecular isodensity surfaces calculated at 0.1 e Å^{-3} obtained by PM3 calculations for the two ions.

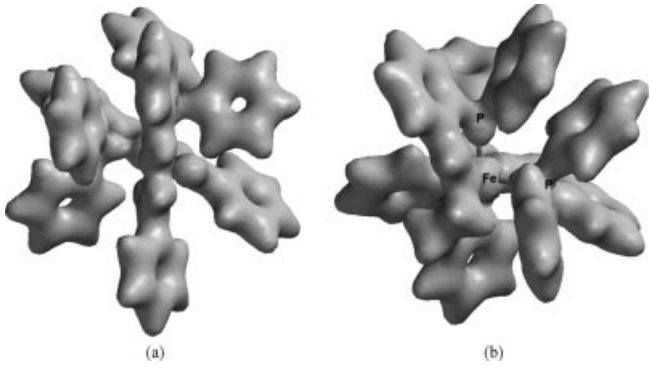

Figure 6. Molecular isodensity surfaces (obtained from the PM3 calculations) drawn at 0.1 e Å^{-3} for $[Fe\{\kappa^3\text{-}(H)PNO\}_2]^{2+}$ (a) and $[Fe(\kappa^3\text{-}PNN)_2]^{2+}$ (b).

Although the choice of the 0.1-e Å^{-3} value is arbitrary, it is noteworthy that the molecular surface of $[Fe\{\kappa^3\text{-}(H)PNO\}_2]^{2+}$ drawn at the same isodensity value does not show analogous voids. This fact seems to suggest that the higher stability of $[Fe\{\kappa^3\text{-}(H)PNO\}_2]^{2+}$ with respect to that of $[Fe(\kappa^3\text{-}PNN)_2]^{2+}$ could be attributed to the different stability (length) of the Fe–P bond in the two fragments, thus explaining the impossibility of forming the bis-chelate octahedral species containing the PNN ligand.

Conclusions

This work has described the synthesis and full characterisation of a new series of iron complexes containing two different tridentate ligands, namely (H)PNO and PNN. Both molecules behave as *mer*-tridentate ligands towards Fe^{II}, but while the benzoyl hydrazone (H)PNO forms the bis-chelate octahedral cation $[Fe\{\kappa^3\text{-}(H)PNO\}_2]^{n+}$ (n = 2, 3), the Schiff base PNN forms exclusively the neutral trigonal-bipyramidal complex $[Fe(\kappa^3\text{-}PNN)Cl_2]$. The formation of complex **1** from hydrate $FeCl_3$ in primary alcohols is worthy of note. The reduction from Fe^{III} to Fe^{II} occurs with oxidation of the alcohol to the corresponding aldehydes, as demonstrated by treating $FeCl_2$, $FeCl_3$ and (H)PNO in *t*BuOH. The different stoichiometries and geometries originated by the two ligands have been investigated by ab initio calculations in order to compare the relative stability of the structurally characterised cationic fragment $[Fe\{\kappa^3\text{-}(H)PNO\}_2]^{2+}$ and the simulated $[Fe(\kappa^3\text{-}PNN)_2]^{2+}$. The results indicate that the $[Fe(\kappa^3\text{-}PNN)_2]^{2+}$ cation is less stable because, due to the long Fe–P distances, the electron density along these bonds is not enough to stabilize the complex. Thus, although the planarity of the aroyl hydrazone (H)PNO makes the embedding of two ligand molecules to form an octahedral entity possible, the high puckering of the chelation rings generated by PNN does not allow the construction of the same coordination geometry.

Experimental Section

All reactions were performed under an atmosphere of dry nitrogen, unless otherwise stated, employing standard Schlenk techniques. Solvents were dried prior to use and stored under an atmosphere of nitrogen. Elemental analyses (C, H, N, S) were performed with a Carlo Erba Mod. EA 1108 apparatus. IR spectra were recorded with a Nicolet 5PCFT-IR spectrophotometer in the 4000–400 cm^{-1} range from KBr disks. Electronic spectra were recorded in the range 250–1000 nm with a Perkin–Elmer Lambda 25 spectrophotometer, employing quartz cuvettes (d = 1 cm). The concentration of the solutions in acetonitrile was 10^{-7} M. ^{1}H NMR spectra were obtained at 300 K with a Bruker 300 FT spectrometer by using $SiMe_4$ as an internal standard. Low-temperature ^{1}H NMR spectra were recorded with a Bruker AC200 spectrometer operating at 200.13 MHz. Peak positions are quoted relative to tetramethylsilane and were calibrated against the residual solvent resonance. $^{31}P\{^1H\}$ NMR spectra were recorded on the same instrument operating at 81.01 MHz. Chemical shifts were measured relative to external 85% H_3PO_4, with downfield shifts considered positive. CI mass spectra (methane) were collected with a Finnigan SSQ 710, FAB mass spectra with a EVG Autospec M, and ESI mass spectra with a Quattro LC triple quadrupole instrument (Micromass, Manchester, UK) equipped with an electrospray interface and Masslynx v. 3.4 software (Micromass). The nebulizing gas (nitrogen, 99.999% purity) and the desolvation gas (nitrogen, 99.998% purity) were delivered at a flow rate of 80 and 500 L h^{-1}, respectively. ESI mass analyses were performed by operating the mass spectrometer in positive-ion (PI) mode, acquiring mass spectra over the scan range m/z = 100–1300 with a step size of 0.1 Da and a scan time of 1.2 s. The operating parameters of the interface were as follows: source temperature: 70 °C; desolvation temperature: 70 °C; ES(+) voltage: 3.0 kV; cone voltage: 30 and 50 V; rf lens: 0.3 V.

All the magnetic susceptibility measurements were performed with a Cryogenic Ltd. S600 SQUID magnetometer. Measurements were always performed on powder samples contained in a thin Teflon film. Data were corrected for the magnetism of the sample holder, which was independently determined at the same temperature range and field. The underlying diamagnetism of the samples was estimated from Pascal's constants.

The cyclic voltammetry experiments were carried out with a computerized potentiostat (PGSTAT 20, Ecochemie) controlled by customized software (GPES 4.8). All measurements were conducted in dry acetonitrile solutions of the studied compound (10^{-3} M) and tetrabutylammonium hexafluorophosphate (10^{-1} M) as supporting electrolyte. Voltammetric characterisations were conducted in oxygen-free solutions that had been previously purged with N_2 for 5 min. Voltammograms were recorded with a scan rate of 0.1 V s^{-1}. A Pt disk electrode with a surface of 7 mm^2 and a Pt rod electrode were used as working and counter electrodes, respectively. Ag/AgCl/3 M KCl was employed as reference electrode.

The ligands (H)PNO[29] and PNN[12] were synthesised according to literature methods. Anhydrous $FeCl_2$, $FeCl_3{\cdot}6H_2O$ and AgOTf (OTf = triflate) were purchased from Aldrich and used as received.

$[Fe\{\kappa^3\text{-}(H)PNO\}_2]Cl[FeCl_4]$ (1) – Method 1: (H)PNO (150 mg, 0.368 mmol) was dissolved in 20 mL of dichloromethane and added dropwise to an ethanol solution (15 mL) containing $FeCl_2$

(50 mg, 0.394 mmol). The resulting red solution was stirred at room temperature for 3 h, concentrated under vacuum and, after the addition of 20 mL of *n*-hexane, cooled to –18 °C overnight. The deep-red solid thus formed was filtered off, washed with *n*-hexane and dried under vacuum. Crystal data and structure refinement for **1** are shown in Table 3. Yield: 130 mg (50%). M.p. 191 °C (dec.). $^{31}P\{^{1}H\}$ NMR ($CDCl_3$, 233 K): δ = 63.4 ppm (s). IR: $\tilde{\nu}$ = 3255 cm^{-1} (w) (N–H), 1607 (m) (C=O). MS (FAB+): *m*/*z* = 1070 $\{[Fe\{(H)PNO\}_2][FeCl_4]\}^+$, 871 $[Fe\{(H)PNO\}(PNO)]^+$, 463 $[Fe(PNO)]^+$. MS (ESI+): *m*/*z* = 871, 463, 409 $[(H)PNO + H^+]^+$. MS (ESI–): *m*/*z* = 198 $[FeCl_4]^-$. $C_{52}H_{42}Cl_5Fe_2N_4O_2P_2 \cdot 2CH_2Cl_2$ (1275.7): calcd. C 50.82, H 3.61, N 4.39; found C 50.74, H 3.58, N 4.19.

Method 2: $FeCl_3 \cdot 6H_2O$ (90 mg, 0.333 mmol) was dissolved in 15 mL of ethanol and the solution was thermostated at 80 °C. (H)PNO (140 mg, 0.343 mmol) was dissolved in 20 mL of ethanol and added dropwise to the iron-containing solution. The resulting red solution was stirred for 48 h, then the volume was reduced under vacuum. After the addition of 20 mL of *n*-hexane and refrigeration at –18 °C prismatic red crystals suitable for X-ray analysis formed. Yield: 270 mg (73%). M.p. 195 °C (dec.). $C_{52}H_{42}Cl_5Fe_2N_4O_2P_2 \cdot 1/2CH_2Cl_2$ (1148.3): calcd. C 54.90, H 3.74, N 4.88; found C 54.53, H 3.75, N 4.35.

Method 3: $FeCl_2$ (16 mg, 0.130 mmol) and $FeCl_3 \cdot 6H_2O$ (35 mg, 0.130 mmol) were dissolved in 10 mL of methanol. (H)PNO (110 mg, 0.270 mmol) was dissolved in 20 mL of dichloromethane and the two solutions were mixed and stirred at room temperature for 5 h to give a deep-red solution. The solvent was then removed under vacuum and the solid residue redissolved in dichloromethane. After the addition of *n*-hexane and refrigeration at –18 °C, a purple solid was collected. Yield: 140 mg (71%). M.p. 192 °C (dec.). $C_{52}H_{42}Cl_5Fe_2N_4O_2P_2 \cdot CH_2Cl_2$ (1190.78): calcd. C 53.43, H 3.70, N 4.70; found C 53.44, H 3.51, N 4.74.

$[Fe_2\{\kappa^3\text{-}(H)PNO\}_2Cl_6]$ (2): (H)PNO (140 mg, 0.343 mmol) was dissolved in dichloromethane (20 mL) and added dropwise to a *t*BuOH solution (15 mL) of $FeCl_3 \cdot 6H_2O$ (90 mg, 0.343 mmol). The resulting red solution was heated at reflux overnight and the microcrystalline red solid formed was filtered off, washed with *n*-hexane and vacuum dried. Crystal data and structure refinement for **2** are shown in Table 3.Yield: 290 mg (88%). M.p. 214–216 °C. ESI(+) MS: *m*/*z* = 872 $[Fe\{(H)PNO\}(PNO)]^+$. MS (ESI–): *m*/*z* = 198 $[FeCl_4]^-$. $C_{52}H_{42}Cl_6Fe_2N_4O_2P_2$ (1141.29): calcd. C 54.74, H 3.71, N 4.91; found C 55.01, H 3.74, N 4.96.

$[Fe\{\kappa^3\text{-}(H)PNO\}_2]Cl_2$ (3): $FeCl_2$ (40 mg, 0.315 mmol) was dissolved in methanol (15 mL) and the solution was heated at 80 °C. (H)-PNO (280 mg, 0.686 mmol) dissolved in 20 mL of dichloromethane was added, and the resulting red solution stirred for 7 h. The solution was then reduced in volume under vacuum and refrigerated at –18 °C overnight. A microcrystalline red solid was filtered off and washed with *n*-hexane. Yield: 220 mg (74%). M.p. 166–173 °C. Owing to oxidation, irreproducible microanalyses were obtained. IR: $\tilde{\nu}$ = 3220 (w) (NH), 1608 (s) (C=O) cm^{-1}. MS (ESI+): *m*/*z* = 871 $[Fe\{(H)PNO\}(PNO)]^+$.

$[Fe\{\kappa^3\text{-}(H)PNO\}_2][TfO]_2$ (4): $FeCl_2$ (20 mg, 0.157 mmol) was dissolved in 15 mL of methanol, and (H)PNO (100 mg, 0.245 mmol) dissolved in 20 mL of dichloromethane was added. The resulting red solution was stirred at room temperature for a few minutes and then AgOTf (70 mg, 0.273 mmol) was added. After 1 h the precipitated AgCl was filtered off and the remaining red solution stirred overnight. The solvent was then removed under vacuum to give a red solid. Yield: 200 mg (70%). M.p. 167–171 °C. $^{31}P\{^{1}H\}$ NMR ($CDCl_3$, 233 K): δ = 62 ppm (s). IR: $\tilde{\nu}$ = 3441 (w) (N–H), 1605 (s) (C=O), 1296 (s) $(SO_3)_{as}$, 1238 (s) $(CF_3)_s$, 1157 (s) $(CF_3)_{as}$, 1027 (s) $(S=O)_s$ cm^{-1}. MS (ESI+): *m*/*z* = 1022 $\{[Fe\{(H)PNO\}_2][TfO]\}^+$, 871 $[Fe\{(H)PNO\}(PNO)]^+$. $C_{54}H_{42}F_6FeN_4O_8P_2S_2 \cdot CH_2Cl_2$ (1255.79): calcd. C 55.38, H 3.59, N 4.79, S 5.47; found C 55.65, H 3.57, N 4.97, S 5.00.

$[Fe(\kappa^3\text{-}PNO)_2]$ (5): NaOMe (30 mg, 0.564 mmol) was dissolved in the minimum amount of methanol and (H)PNO (230 mg, 0.563 mmol) dissolved in 15 mL of dichloromethane was added. $FeCl_2$ (35 mg, 0.282 mmol) was then added and the deep-red solution thus obtained was stirred at room temperature for 48 h. After partial removal of the solvent under vacuum, a red solid was filtered off and washed with *n*-hexane. Yield: 200 mg (80%). M.p. 193–196 °C. ^{1}H NMR ($CDCl_3$, 233 K): δ = 9.60 (s, 1 H, CH=N), 7.68–6.80 (m, 19 H, Ph) ppm. $^{31}P\{^{1}H\}$ NMR ($CDCl_3$, 233 K): δ = 69.2 (s) ppm. MS (CI+): *m*/*z* = 871 $[\mathbf{5} + H^+]^+$.

Table 3. Crystal data and structure refinement for **1**, **2** and **6**.

	1	**2**	**6**
Empirical formula	$C_{52}H_{42}Cl_5Fe_2N_4O_2P_2$	$C_{52}H_{42}Cl_{5.4}Fe_2N_4O_2P_2$	$C_{26.5}H_{24}Cl_3FeN_2P$
Formula weight	1105.79	1119.97	563.65
Wavelength [Å]	0.71073	0.71073	0.71073
Crystal system	monoclinic	monoclinic	monoclinic
Space group	$P2_1/c$	$P2_1/n$	$C2/c$
a [Å]	17.541(3)	14.0974(8)	38.884(3)
b [Å]	13.665(3)	21.446(1)	18.1301(5)
c [Å]	21.882(4)	18.440(1)	16.890(1)
β [°]	96.431(3)	93.081(1)	101.153(1)
Volume [$Å^3$]	5212.1(17)	5567.0(5)	5238.6(6)
Z	4	4	8
Density (calculated) [$Mg\,m^{-3}$]	1.409	1.336	1.429
Absorption coefficient [mm^{-1}]	0.918	0.879	0.961
F(000)	2260	2287	2312
θ range for data collection [°]	1.76–18.86	1.46–24.73	1.07–26.38
Independent reflections	4052 [*R*(int) = 0.1019]	9511 [*R*(int) = 0.0353]	5361 [*R*(int) = 0.0235]
Data/restraints/parameters	4052/9/540	9511/1/667	5361/3/305
Goodness-of-fit on F^2	1.262	1.443	1.086
Final *R* indices [$I > 2\sigma(I)$] (R_1, wR_2)	0.0946, 0.1775	0.1039, 0.3185	0.0545, 0.1806
R indices (all data) (R_1, wR_2)	0.1317, 0.1985	0.1299, 0.3518	0.0657, 0.1910
Final ΔF max./min. [$e\,Å^{-3}$]	0.436/–0.425	2.577/–0.532	1.616/–0.854

$C_{52}H_{42}FeN_4O_2P_2 \cdot 2CH_3OH$ (936.81): calcd. C 69.23, H 5.34, N 5.98; found C 69.47, H 4.88, N 5.46.

[Fe(κ³-PNN)Cl₂] (6): $FeCl_2$ (40 mg, 0.331 mmol) was dissolved in methanol (15 mL) and a dichloromethane solution (20 mL) of PNN (130 mg, 0.330 mmol) was added dropwise at room temperature. After 24 h of stirring the orange solid formed was removed by filtration while the remaining solution was dried under vacuum to give a light red solid. This solid was dissolved in dichloromethane (10 mL) and the clear solution was added to *n*-hexane (10 mL) and then cooled overnight at –18 °C. Orange crystals suitable for X-ray analysis were collected. Crystal data and structure refinement for **6** are shown in Table 3.Yield: 120 mg (70%). M.p. 86–90 °C. IR: $\tilde{\nu}$ = 1629 (s) (C=N) cm^{-1}. MS (FAB+): *m/z* = 563 $[\mathbf{6}]^+$. $C_{26}H_{23}Cl_2FeN_2P \cdot 1/2CH_2Cl_2$ (563.68): calcd. C 56.47, H 4.29, N 4.97; found C 56.94, H 4.26, N 4.60.

X-ray Analysis: Mo-*Kα* radiation (λ = 0.71073 Å), *T* = 293 K for all compounds (SMART AXS 1000 CCD diffractometer). Lorentz, polarization, and absorption corrections were applied.[30] Structures solved by direct methods by using SIR97[31] and refined by full-matrix least-squares on all F^2 by using SHELXL97[32] implemented in the WingX package.[33] Hydrogen atoms partly located on Fourier difference maps and refined isotropically and partly introduced in calculated positions. Anisotropic displacement parameters refined for all non-hydrogen atoms. In **6** a partially occupied (50%) CH_2Cl_2 molecule is found in the asymmetric unit, with traces of residual electron density around the central carbon in the final map. Compound **2**, with stoichiometry $[Fe_2\{\kappa^3\text{-}(H)\text{-}PNO\}_2Cl_6]$, shows substitutional disorder which has been modelled as a replacement between $[FeCl_5]^2$- and $[FeCl_4]^2$- anions; the poor quality of diffraction data, however, did not allow for the establishment of an accurate description of the disordered entities, and quite high electron density residuals were present in the final maps in the disordered region. Molecular and crystal geometries have been analyzed with SHELXL97[32] and PARST97[34], and extensive use was made of the Cambridge Crystallographic Data Centre packages[35]. Table 3 summarizes crystal data and structure determination results. CCDC-616781 (for **1**), -616782 (for **2**) and -616783 (for **3**) contain the supplementary crystallographic data for this paper. These data can be obtained free of charge from The Cambridge Crystallographic Data Centre via www.ccdc.cam.ac.uk/data_request/cif.

Acknowledgments

Prof. Maria Carmen Rodriguez Argüelles (University of Vigo, Spain) is thanked for the FAB-MS analyses, while Dr. Elisa Elviri (University of Parma) is thanked for the ESI-MS analyses. The authors wish to thank the C.I.M. (Centro Interfacoltà di Misure G. Casnati) of the University of Parma for the instrument facilities.

[1] a) V. C. Gibson, S. K. Spitzmesser, *Chem. Rev.* **2003**, *103*, 283–315; b) S. D. Ittel, L. K. Johnson, M. Brookhart, *Chem. Rev.* **2000**, *100*, 1169–1203.
[2] R. K. O'Reilly, V. C. Gibson, A. J. P. White, D. J. Williams, *J. Am. Chem. Soc.* **2003**, *125*, 8450–8451.
[3] G. Müller, M. Klinga, B. Rieger, *Z. Anorg. Allg. Chem.* **2002**, *628*, 2839–2846.
[4] L. H. Uppadine, J. M. Lehn, *Angew. Chem. Int. Ed.* **2004**, *43*, 240–243.
[5] H. Torigoe, H. Hagiwara, S. Arata, M. Yamada, N. Matsumoto, *Chem. Lett.* **2005**, *34*, 956–957.
[6] M. Velusamy, R. Mayilmurugan, M. Palaniandavar, *J. Inorg. Biochem.* **2005**, *99*, 1032–1042.
[7] T. C. Harrop, M. M. Olmstead, P. K. Mascharak, *Inorg. Chem.* **2005**, *44*, 9527–9533.
[8] J. Legros, C. Bolm, *Chem. Eur. J.* **2005**, *11*, 1086–1092.
[9] a) P. Pelagatti, A. Bacchi, C. Bobbio, M. Carcelli, M. Costa, C. Pelizzi, C. Vivorio, *Organometallics* **2000**, *19*, 5440–5446; b) A. Bacchi, M. Carcelli, M. Costa, A. Fochi, C. Monici, P. Pelagatti, C. Pelizzi, G. Pelizzi, L. M. Sanjuan Roca, *J. Organomet. Chem.* **2000**, *593–594*, 180–191; c) P. Pelagatti, M. Carcelli, F. Franchi, C. Pelizzi, A. Bacchi, A. Fochi, H.-W. Frühauf, K. Goubitz, K. Vrieze, *Eur. J. Inorg. Chem.* **2000**, 463–475; d) P. Pelagatti, A. Bacchi, C. Bobbio, M. Carcelli, M. Costa, A. Fochi, C. Pelizzi, *J. Chem. Soc., Dalton Trans.* **2002**, 1820–1825; e) P. Pelagatti, A. Vergnani, M. Carcelli, M. Costa, D. Rogolino, A. Bacchi, C. Pelizzi, *Inorg. Chim. Acta* **2003**, *351*, 235–241; f) P. Pelagatti, A. Bacchi, M. Carcelli, M. Costa, H.-W. Frühauf, K. Goubitz, C. Pelizzi, M. Triclistri, K. Vrieze, *Eur. J. Inorg. Chem.* **2002**, 139–446; g) A. Bacchi, M. Carcelli, C. Pelizzi, G. Pelizzi, P. Pelagatti, S. Ugolotti, *Eur. J. Inorg. Chem.* **2002**, 2179–2187.
[10] a) P. Pelagatti, A. Venturini, A. Leporati, M. Carcelli, M. Costa, A. Bacchi, G. Pelizzi, C. Pelizzi, *J. Chem. Soc., Dalton Trans.* **1998**, 2715–2721; b) P. Pelagatti, A. Bacchi, M. Carcelli, M. Costa, A. Fochi, P. Ghidini, E. Leporati, M. Masi, C. Pelizzi, G. Pelizzi, *J. Organomet. Chem.* **1999**, *583*, 94–105; c) M. Costa, P. Pelagatti, C. Pelizzi, D. Rogolino, *J. Mol. Catal. A* **2002**, *178*, 21–26.
[11] P. Pelagatti, A. Bacchi, M. Balordi, S. Bolaño, F. Calbiani, L. Elviri, L. Gonsalvi, C. Pelizzi, M. Peruzzini, D. Rogolino, *Eur. J. Inorg. Chem.* **2006**, 2422–2436.
[12] R. E. Rülke, V. E. Kaasjager, P. Wehman, C. J. Elsevier, P. W. N. M. van Leeuwen, K. Vrieze, J. Fraanje, K. Goubitz, A. L. Spek, *Organometallics* **1996**, *15*, 3022–3031.
[13] a) P. V. Bernhardt, P. Chin, D. R. Richardson, *J. Biol. Inorg. Chem.* **2001**, *6*, 801–809; b) C. M. Armstrong, P. V. Bernhardt, P. Chin, D. S. Richardson, *Eur. J. Inorg. Chem.* **2003**, 1145–1156; c) P. V. Bernhardt, L. M. Caldwell, T. B. Chaston, P. Chin, D. R. Richardson, *J. Biol. Inorg. Chem.* **2003**, *8*, 866–880.
[14] G. J. P. Britovsek, V. C. Gobson, B. S. Kimberley, S. Mastroianni, C. Redshaw, G. A. Solan, A. J. P. White, D. J. Williams, *J. Chem. Soc., Dalton Trans.* **2001**, 1639–1644.
[15] J. E. Dubois, H. Fakhrayan, J.-P. Doucet, J.-M. El H. Chahine, *Inorg. Chem.* **1992**, *31*, 853–859.
[16] a) M. Di Vaira, F. Mani, P. Stoppioni, *J. Chem. Soc., Dalton Trans.* **1997**, 1375–1379; b) C. A. Clausen, M. L. Good, *Inorg. Chem.* **1970**, *9*, 220–223.
[17] a) D. Onggo, A. D. Rae, H. A. Goodwin, *Inorg. Chim. Acta* **1990**, *178*, 151–163; b) S. E. Livingstone, J. D. Nolan, *J. Chem. Soc., Dalton Trans.* **1972**, 218–223.
[18] a) O. Schramel, B. Michalke, A. Kettrup, *J. Chromatogr. A* **1998**, *819*, 231–242; b) G. Weber, N. von Wirén, H. Hayen, *Rapid Commun. Mass Spectrom.* **2006**, *20*, 973–980.
[19] D. H. Johnston, D. F. Shriver, *Inorg. Chem.* **1993**, *32*, 1045–1047.
[20] J. Wang, F. R. Keene, *Electrochim. Acta* **1996**, *41*, 2563–2569, and references cited therein.
[21] a) F. Benvenuti, C. Carlini, M. Marchionna, R. Patrini, A. M. Raspolli Galletti, G. Sbrana, *J. Mol. Catal. A* **1999**, *140*, 139–155; b) L. Canovese, F. Visentin, G. Chessa, A. Niero, P. Uguagliati, *Inorg. Chim. Acta* **1999**, *293*, 44–52.
[22] J.-P. Masson, A. A. Bahsoun, M.-T. Youinou, J. A. Osborn, *C. R. Chim.* **2002**, *5*, 303–308.
[23] a) C.-C. Yang, W.-Y. Yeh, G.-H. Lee, S.-M. Peng, *J. Organomet. Chem.* **2000**, *598*, 353–358; b) M. E. Bluhm, O. Walter, M. Döring, *J. Organomet. Chem.* **2005**, *690*, 713–721.
[24] W.-Y. Yeh, C.-C. Yang, S.-M. Peng, G.-H. Lee, *J. Chem. Soc., Dalton Trans.* **2000**, 1649–1654.
[25] D. Cremer, J. A. Pople, *J. Am. Chem. Soc.* **1975**, *97*, 1354–1358.

[26] P. Wehman, R. E. Rülke, V. E. Kaasjager, P. C. J. Kamer, H. Kooijman, A. L. Spek, C. J. Elsevier, K. Vrieze, P. W. N. M. van Leeuwen, *J. Chem. Soc., Chem. Commun.* **1995**, 331–332.
[27] a) J. J. P. Stewart, *J. Comput. Chem.* **1989**, *10*, 209; b) J. J. P. Stewart, *J. Comput. Chem.* **1989**, *10*, 221.
[28] Spartan 04, Release 1.01, **2004**, Wavefunction, Inc., 18401 Von Karman Avenue, Suite 370, Irvine, Ca 92612 USA (http://www.wavefun.com).
[29] A. Bacchi, M. Carcelli, M. Costa, P. Pelagatti, C. Pelizzi, G. Pelizzi, *Gazz. Chim. Ital.* **1994**, *124*, 429–435.
[30] a) SAINT: SAX, Area Detector Integration, Siemens Analytical instruments Inc., Madison, Wisconsin, USA; b) G. Sheldrick, *SADABS: Siemens Area Detector Absorption Correction Software*, **1996**, University of Göttingen, Germany.
[31] A. Altomare, M. C. Burla, M. Cavalli, G. Cascarano, C., Giacovazzo, A. Gagliardi, A. G. Moliterni, G. Polidori, R. Spagna, *Sir97: A New Program for Solving and Refining Crystal Structures* **1997**, Istituto di Ricerca per lo Sviluppo di Metodologie Cristallografiche CNR, Bari.
[32] G. Sheldrick, *SHELXL97: Program for Structure Refinement*, University of Göttingen, Germany, **1997**.
[33] L. J. Farrugia, *J. Appl. Crystallogr.* **1999**, *32*, 837–838.
[34] M. Nardelli, *J. Appl. Crystallogr.* **1995**, *28*, 659.
[35] a) F. H. Allen, O. Kennard, R. Taylor, *Acc. Chem. Res.* **1983**, *16*, 146–153; b) I. J. Bruno, J. C. Cole, P. R. Edgington, M. Kessler, C. F. Macrae, P. McCabe, J. Pearson, R. Taylor, *Acta Crystallogr. Sect. B* **2002**, *58*, 389–397.

Received: August 4, 2006
Published Online: November 27, 2006

